Chapter 10

Towards the Description of Covalent Bonds in Subsystem Density-Functional Theory

Christoph R. Jacob[1] and Lucas Visscher[2]

[1] *Karlsruher Institut für Technolgie (KIT)*
Center for Functional Nanostructures
Wolfgang-Gaede-Str. 1a, 76131 Karlsruhe, Germany
christoph.jacob@kit.edu

[2] *VU University Amsterdam*
Amsterdam Center for Multiscale Modeling
De Boelelaan 1083, 1081 HV Amsterdam, The Netherlands
visscher@chem.vu.nl

Current applications of frozen-density embedding (FDE)—or more generally subsystem density-functional theory (DFT) schemes—are limited to subsystems that are not connected by covalent bonds. This restriction is due to the insufficiencies of the available approximate kinetic-energy functionals, which are used to calculate the contribution of the nonadditive kinetic energy to the effective embedding potential. In this Chapter, we discuss two different approaches to overcome these limitations and to extend the applicability of the FDE scheme to subsystems connected by covalent bonds. First, we outline possibilities to improve the currently available approximations applied for the kinetic-energy component of the embedding potential. Second, we show how a generalized three-partition FDE scheme can be employed to circumvent the problems in the approximate kinetic-energy functionals by introducing capping groups, thus allowing for a subsystem DFT treatment of proteins.

Contents

10.1. Introduction

The accurate quantum chemical treatment of large systems, such as biomolecules (e.g., proteins) or condensed phase systems (e.g., transition metal catalysts in solution, molecules interacting with surfaces, or impurities in crystals), presents a significant challenge for theoretical chemistry (see, e.g., Refs. 1–4). In particular, two main problems have to be overcome. First, the required computational effort increases with the size of the studied system, which puts a significant burden on an accurate treatment of large systems. This first problem can be addressed by using efficient computational methods, mostly based on density-functional theory (DFT), which show a linear scaling of the required computer time with the size of the system.[5,6] However, a second problem remains. For full quantum-chemical calculations on large systems, a large amount of data is obtained, which hampers the interpretation of the results and makes it difficult to extract general conclusions from such calculations (see, e.g., Refs. 7 and 8, where this problem is discussed in the context of theoretical vibrational spectroscopy).

Subsystem approaches, in which the full system is decomposed into its constituting fragments that are then each treated individually (for examples, see Refs. 9–15), offer a very attractive alternative to a treatment of the full system. First, subsystem methods are in general more efficient than a conventional treatment, since the computer time required for the calculation of one subsystem is usually independent of the size of the full system, so that one naturally obtains a linear scaling of the computational effort with the size of the system.[9–11] Second, a partitioning into subsystems provides a more natural way for the interpretation of the results, since it offers a picture in terms of the chemical building blocks of the system such as, e.g., the individual molecules in a condensed phase system or the amino acid residues constituting a protein. Finally, subsystem approaches provide the possibility to focus on interesting parts of the system, such as the active site of an enzyme or of another catalyst, solute molecules in a liquid phase, absorbed molecules on surfaces, or impurities in crystals. Since the subsystems are treated individually, it is easily possible to employ a more accurate treatment only for one or a few selected subsystems of interest or to introduce additional approximations for subsystems that are less important.[16–18] In particular, such a subsystem description makes it possible to apply a wave-function theory (WFT) description to one subsystem, while its environment is treated more efficiently using DFT.[19–24]

A very appealing subsystem approach is offered by the frozen-density embedding (FDE) scheme within DFT introduced by Wesolowski and Warshel.[16,25] In this FDE scheme, the total electron density is partitioned into possibly overlapping electron densities of an active subsystem and of a frozen environment, and the

electron density of the active subsystem is optimized in the presence of the frozen environment. The effect of the frozen environment on the active subsystem is included by the use of an effective embedding potential, that contains in addition to the electrostatic potential of the nuclei in the environment and the Coulomb potential of the electron density of the environment, also a component of the nonadditive exchange–correlation energy and of the nonadditive kinetic energy.[16,25]

The FDE scheme is based on a more general subsystem formulation of DFT by Cortona,[9] in which the electron densities of an arbitrary number of subsystems are each optimized individually. Such a general subsystem DFT scheme makes it possible to employ different levels of approximations for different parts of the system.[18] Compared to other subsystem approaches, the FDE scheme offers the advantages that it includes the effect of the environment in an accurate and improvable way,[18,26,27] and that it provides a exact treatment in the exact functional limit.[25]

However, the FDE scheme relies on the use of an approximate functional for the nonadditive kinetic energy and the corresponding component of the effective embedding potential and its applicability is, therefore, limited by the quality of the available approximate functionals. While it has been shown that with the available generalized-gradient approximation (GGA) kinetic-energy functionals, in particular the PW91k functional,[28] accurate results can be obtained for van der Waals complexes[29–31] and hydrogen-bonded complexes,[32–34] FDE currently cannot be applied to subsystems connected by covalent bonds.

While for the description of liquid phase systems such as solvated molecules a partitioning into the individual solute and solvent molecules is possible and a description of covalent bonds between subsystems is not necessary, there are several important areas of application where a subsystem description would require the treatment of covalent bonds between subsystems. For instance, the theoretical modeling of biologically relevant systems, e.g., proteins or their active centers, naturally leads to a partitioning into individual amino acid residues (or of larger subunits) connected by covalent bonds. Similarly, a subsystem description of larger transition metal complexes in solution would benefit from the possibility to describe the active center and the ligands of the catalysts as separate subsystems.

Therefore, further theoretical developments are required to make applications of FDE or more generally subsystem DFT possible for such systems. In this Chapter, we give an overview of recent work addressing these problems. In Sec. 10.2, we present the theoretical background of FDE and subsystem DFT. This is followed by the discussion of different approaches for the description of covalent bonds within FDE and subsystem DFT. In Sec. 10.3, we begin with reviewing some recent developments of improved approximations to the kinetic-energy component of the embedding potential and we discuss their relevance for the description of covalent bonds. In Sec. 10.4, we show how the insufficiencies in the available approximate kinetic-energy functionals can be circumvented by the introduction of

capping groups in a three-partition FDE scheme, and how such a scheme can be applied to the description of proteins. Finally, concluding remarks are given and possible directions for future developments are outlined in Sec. 10.5.

10.2. Theoretical background

10.2.1. *Frozen-density embedding*

The FDE scheme[16,25] is based on a partitioning of the total electron density $\rho_{\mathrm{tot}}(\boldsymbol{r})$ into the electron densities of two subsystems, i.e., $\rho_{\mathrm{tot}}(\boldsymbol{r})$ is represented as the sum of two components $\rho_{\mathrm{I}}(\boldsymbol{r})$ and $\rho_{\mathrm{II}}(\boldsymbol{r})$,

$$\rho_{\mathrm{tot}}(\boldsymbol{r}) = \rho_{\mathrm{I}}(\boldsymbol{r}) + \rho_{\mathrm{II}}(\boldsymbol{r}). \tag{10.2.1}$$

Except for the requirement that both subsystem densities integrate to an integer number of electrons, they are not subject to any further conditions. In particular, the subsystem densities are allowed to overlap. In addition to the electron density, the nuclear charges are partitioned accordingly. This partitioning of the density and of the nuclear charges defines two subsystems (subsystems I and II).

Given this partitioning, the DFT total energy can (in the absence of any external fields) be expressed as a functional of ρ_{I} and ρ_{II},

$$\begin{aligned} E[\rho_{\mathrm{I}}, \rho_{\mathrm{II}}] = E_{\mathrm{NN}} &+ \int \big(\rho_{\mathrm{I}}(\boldsymbol{r}) + \rho_{\mathrm{II}}(\boldsymbol{r})\big)\big(v_{\mathrm{I}}^{\mathrm{nuc}}(\boldsymbol{r}) + v_{\mathrm{II}}^{\mathrm{nuc}}(\boldsymbol{r})\big)\, d\boldsymbol{r} \\ &+ \frac{1}{2}\int \frac{\big(\rho_{\mathrm{I}}(\boldsymbol{r}) + \rho_{\mathrm{II}}(\boldsymbol{r})\big)\big(\rho_{\mathrm{I}}(\boldsymbol{r'}) + \rho_{\mathrm{II}}(\boldsymbol{r'})\big)}{|\boldsymbol{r} - \boldsymbol{r'}|}\, d\boldsymbol{r} d\boldsymbol{r'} \\ &+ E_{xc}[\rho_{\mathrm{I}} + \rho_{\mathrm{II}}] + T_s[\rho_{\mathrm{I}}] + T_s[\rho_{\mathrm{II}}] + T_s^{\mathrm{nadd}}[\rho_{\mathrm{I}}, \rho_{\mathrm{II}}], \end{aligned} \tag{10.2.2}$$

where E_{NN} is the nuclear repulsion energy, $v_{\mathrm{I}}^{\mathrm{nuc}}$ and $v_{\mathrm{II}}^{\mathrm{nuc}}$ are the electrostatic potentials of the nuclei in subsystems I and II, respectively, E_{xc} is the exchange–correlation energy functional, $T_s[\rho]$ is the kinetic energy of the noninteracting reference system, and $T_s^{\mathrm{nadd}}[\rho_{\mathrm{I}}, \rho_{\mathrm{II}}]$ is the nonadditive kinetic energy, which is defined as

$$T_s^{\mathrm{nadd}}[\rho_{\mathrm{I}}, \rho_{\mathrm{II}}] = T_s[\rho_{\mathrm{I}} + \rho_{\mathrm{II}}] - T_s[\rho_{\mathrm{I}}] - T_s[\rho_{\mathrm{II}}]. \tag{10.2.3}$$

The densities $\rho_{\mathrm{I}}(\boldsymbol{r})$ and $\rho_{\mathrm{II}}(\boldsymbol{r})$ can be represented using the canonical Kohn–Sham (KS) orbitals for the individual subsystems $\phi_i^{(n)}$ with

$$\rho_n(\boldsymbol{r}) = 2 \sum_{i=1}^{N_n/2} \left|\phi_i^{(n)}(\boldsymbol{r})\right|^2, \tag{10.2.4}$$

where $n = \mathrm{I}, \mathrm{II}$ denotes the considered subsystem and N_{I} and N_{II} denote the number of electrons in subsystems I and II, respectively. For reasons of simplicity, only the closed-shell case with $N_n/2$ doubly occupied KS orbitals in each subsystem will be considered. A generalization to open-shell systems is possible in a straightforward

way.[35] Using the KS orbitals, it is possible to calculate the kinetic energy of the corresponding noninteracting reference system as

$$T_s[\rho_n] = -\sum_{i=1}^{N_n/2} \int \phi_i^{(n)}(\boldsymbol{r}) \nabla^2 \phi_i^{(n)}(\boldsymbol{r})\, d\boldsymbol{r}. \tag{10.2.5}$$

However, with the partitioning of the total electron density into $\rho_{\mathrm{I}}(\boldsymbol{r})$ and $\rho_{\mathrm{II}}(\boldsymbol{r})$ there is in general no representation of $\rho_{\mathrm{tot}}(\boldsymbol{r})$ in the canonical KS orbitals available, so that $T_s[\rho_{\mathrm{I}} + \rho_{\mathrm{II}}]$ cannot be calculated in this way. Therefore, in practical implementations $T_s^{\mathrm{nadd}}[\rho_{\mathrm{I}}, \rho_{\mathrm{II}}]$ has to be approximated (see Sec. 10.2.4).

For a given frozen electron density $\rho_{\mathrm{II}}(\boldsymbol{r})$ in one of the subsystems (subsystem II) the electron density $\rho_{\mathrm{I}}(\boldsymbol{r})$ in the other subsystem (subsystem I) can be determined by minimizing the total energy bifunctional [Eq. (10.2.2)] with respect to ρ_{I}, while $\rho_{\mathrm{II}}(\boldsymbol{r})$ is kept frozen. If the complementary $\rho_{\mathrm{I}}(\boldsymbol{r})$ is positive, this will lead to the total density $\rho_{\mathrm{tot}}(\boldsymbol{r}) = \rho_{\mathrm{I}}(\boldsymbol{r}) + \rho_{\mathrm{II}}(\boldsymbol{r})$ that minimizes the total energy functional. This total density is, therefore, the same density that could also be obtained from a conventional DFT calculation on the total system.

The minimization of the total energy $E[\rho_{\mathrm{I}}, \rho_{\mathrm{II}}]$ with respect to ρ_{I}, under the constraint that the number of electrons N_{I} in subsystem I is conserved, leads to a set of Kohn–Sham-like equations for the KS orbitals of subsystem I (where it has to be assumed that the exact ρ_{I} is v_s-representable),

$$\left[-\frac{\nabla^2}{2} + v_{\mathrm{eff}}^{\mathrm{KSCED}}[\rho_{\mathrm{I}}, \rho_{\mathrm{II}}](\boldsymbol{r})\right] \phi_i^{(\mathrm{I})}(\boldsymbol{r}) = \epsilon_i\, \phi_i^{(\mathrm{I})}(\boldsymbol{r}); \quad i = 1, \ldots, N_{\mathrm{I}}/2, \tag{10.2.6}$$

which are usually referred to as *Kohn–Sham equations with constraint electron density (KSCED equations)*.

In these equations, the KSCED effective potential is given by

$$v_{\mathrm{eff}}^{\mathrm{KSCED}}[\rho_{\mathrm{I}}, \rho_{\mathrm{II}}](\boldsymbol{r}) = v_{\mathrm{eff}}^{\mathrm{KS}}[\rho_{\mathrm{I}}](\boldsymbol{r}) + v_{\mathrm{eff}}^{\mathrm{emb}}[\rho_{\mathrm{I}}, \rho_{\mathrm{II}}](\boldsymbol{r}), \tag{10.2.7}$$

where $v_{\mathrm{eff}}^{\mathrm{KS}}[\rho_{\mathrm{I}}](\boldsymbol{r})$ is the KS effective potential of the isolated subsystem I containing the usual terms of the nuclear potential, the Coulomb potential of the electrons, and the exchange–correlation potential,

$$v_{\mathrm{eff}}^{\mathrm{KS}}[\rho_{\mathrm{I}}](\boldsymbol{r}) = v_{\mathrm{I}}^{\mathrm{nuc}}(\boldsymbol{r}) + \int \frac{\rho_{\mathrm{I}}(\boldsymbol{r'})}{|\boldsymbol{r} - \boldsymbol{r'}|} d\boldsymbol{r'} + \left.\frac{\delta E_{\mathrm{xc}}[\rho]}{\delta \rho}\right|_{\rho=\rho_{\mathrm{I}}(\boldsymbol{r})}, \tag{10.2.8}$$

and the effective embedding potential $v_{\mathrm{eff}}^{\mathrm{emb}}[\rho_{\mathrm{I}}, \rho_{\mathrm{II}}](\boldsymbol{r})$ describes the interaction of the subsystem I with the frozen density and nuclei of subsystem II and reads

$$\begin{aligned} v_{\mathrm{eff}}^{\mathrm{emb}}[\rho_{\mathrm{I}}, \rho_{\mathrm{II}}](\boldsymbol{r}) = v_{\mathrm{II}}^{\mathrm{nuc}}(\boldsymbol{r}) + \int \frac{\rho_{\mathrm{II}}(\boldsymbol{r'})}{|\boldsymbol{r} - \boldsymbol{r'}|} d\boldsymbol{r'} \\ + \left.\frac{\delta E_{\mathrm{xc}}[\rho]}{\delta \rho}\right|_{\rho=\rho_{\mathrm{I}}+\rho_{\mathrm{II}}} - \left.\frac{\delta E_{\mathrm{xc}}[\rho]}{\delta \rho}\right|_{\rho=\rho_{\mathrm{I}}} + v_T[\rho_{\mathrm{I}}, \rho_{\mathrm{II}}](\boldsymbol{r}). \end{aligned} \tag{10.2.9}$$

In addition to the electrostatic potential of the nuclei and the electrons in the frozen subsystem, this effective embedding potential also contains an exchange–correlation component and a kinetic-energy component $v_T[\rho_\mathrm{I}, \rho_\mathrm{II}]$ which is given as the functional derivative of the nonadditive kinetic-energy bifunctional,

$$v_T[\rho_\mathrm{I}, \rho_\mathrm{II}](\boldsymbol{r}) = \frac{\delta T_s^\mathrm{nadd}[\rho_\mathrm{I}, \rho_\mathrm{II}]}{\delta \rho_\mathrm{I}} = \left.\frac{\delta T_s[\rho]}{\delta \rho}\right|_{\rho=\rho_\mathrm{tot}(\boldsymbol{r})} - \left.\frac{\delta T_s[\rho]}{\delta \rho}\right|_{\rho=\rho_\mathrm{I}(\boldsymbol{r})} . \quad (10.2.10)$$

In practical applications of the FDE scheme, this kinetic-energy component v_T has to be approximated (see Sec. 10.2.4). Note that for GGA exchange–correlation functionals no additional approximations have to be introduced for the exchange–correlation component of the embedding potential, but when using orbital-dependent exchange–correlation functionals, additional approximations have to be introduced in the exchange–correlation component of the embedding potential.[31]

For a given frozen density $\rho_\mathrm{II}(\boldsymbol{r})$, the density of the nonfrozen subsystem $\rho_\mathrm{I}(\boldsymbol{r})$ can be obtained by solving the above KSCED equations with the embedding potential $v_\mathrm{eff}^\mathrm{emb}$ as given in Eq. (10.2.9). If the initial assumption that the complementary ρ_I is positive and v_s-representable is fulfilled, the solution of these equations will directly yield the exact ground-state electron density of the total system.[25]

In typical applications of the FDE scheme, the nonfrozen subsystem I is a small system of interest, which is embedded in a much larger environment. Especially for the calculation of molecular properties (e.g., electronic excitation energies, or nuclear magnetic resonance shieldings), this will be a very efficient scheme, since the property calculation generally has to be performed for the nonfrozen subsystem only. However, in these cases the construction of the electron density of the frozen environment becomes a bottleneck if the standard approach is used and the frozen density is obtained using a DFT calculation of the full environment.

This problem can be overcome by applying approximations in the construction of the environment density, because Eq. (10.2.6) can be solved for any postulated electron density, so that $\rho_\mathrm{II}(\boldsymbol{r})$ may also be obtained from simpler considerations. Already in their initial papers, Wesolowski and Warshel proposed the use of such an approximate density to describe a water environment.[16,36] In a study of solvent effects on excitation energies, Neugebauer *et al.* investigated the electronic absorption spectrum of acetone in water and tested different approximate descriptions of the frozen solvent environment. They found that compared to a full DFT calculation of the environment, the error introduced by using a superposition of densities of isolated water molecules is less than 0.01 eV for the $n \to \pi^*$ transition of interest. Subsequently, this strategy has been successfully applied in a number of studies of solvent effects on molecular properties.[26,37–39]

10.2.2. *Subsystem DFT*

While the strategy to use fixed approximate densities as described in the previous

section can be applied for large environments, the FDE formalism can also be used to determine the electron densities of both subsystems. In particular, for most approximate environment densities, the requirements that the complementary ρ_{I} is v_s-representable and positive at any point in space will not be fulfilled. To correct for the errors introduced by these deficiencies of the approximate environment density, both the electron density in the nonfrozen subsystem and the environment density should be adjusted. This leads to the "subsystem DFT" formalism as it was initially proposed by Cortona,[9] which provides an alternative to conventional KS-DFT.

The starting point for this subsystem DFT formulation is again the total energy bifunctional of Eq. (10.2.2), but now this total energy is not only minimized with respect to the electron density ρ_{I} in one of the subsystems while the density ρ_{II} in the other subsystem is kept frozen, but it is minimized with respect to the electron densities in both subsystems. This leads to a set of two coupled sets of KSCED equations, which have to be solved self-consistently. This can be done by applying so-called "freeze-and-thaw" cycles,[27] in which the roles of frozen and nonfrozen subsystem are interchanged until convergence is reached.

10.2.3. *Extension to many subsystems and multilevel simulations*

The subsystem DFT scheme can be easily extended to an arbitrary number of subsystems by starting from the partitioning

$$\rho_{\mathrm{tot}}(\boldsymbol{r}) = \sum_{i=1}^{M} \rho_i(\boldsymbol{r}), \tag{10.2.11}$$

where M is the number of subsystems. This leads to a formulation similar to the one presented above, except that a set of M coupled KSCED equations is obtained, in which the frozen density in the effective embedding potential is replaced by the sum of the densities of all frozen subsystems.[9,10] This set of equations can be either solved iteratively using freeze-and-thaw cycles,[27] or alternatively, the coupled KSCED equations can be solved simultaneously by updating all densities after each SCF cycle.[10,11]

This generalized subsystem DFT approach, in which the densities of all subsystems are optimized, can be used as an alternative to conventional KS-DFT calculation for large systems. By construction, it scales linearly with the number of subsystems. Initially, it has been applied by Cortona and co-workers for calculations on simple ionic crystals (e.g., alkali halides,[40] alkali-earth oxides,[41] and alkali-earth sulfides[42]) by determining the densities of the ions individually. While in the implementation of Cortona, these densities were constrained to be spherical, an extended scheme has been implemented by Mehl and co-workers. They allow deformations of the atomic densities, and studied alkali halides[43] and corundum.[44]

This subsystem DFT approach has been implemented by Iannuzzi *et al.* in the CP2K program package.[10] With their implementation molecular dynamics simulations can be performed, in which the individual molecules are treated as sub-

systems. Another implementation has been presented by Shimojo *et al.*, who also implemented a similar subsystem DFT scheme in combination with a numerical integration algorithm employing hierarchical real-space grids as an efficient alternative to standard KS-DFT calculations.[11] They have applied their implementation to MD simulations of aluminum nanoparticles and of nanoindentation of ceramics materials.[45]

The implementation in the ADF program package[18,37] supports the general subsystem DFT approach, in which the densities of an arbitrary number of subsystems are each optimized iteratively. On the other hand, it is also possible to optimize only the density of one active subsystem, while all other subsystems form a frozen environment, leading to the FDE scheme. Furthermore, the implementation also allows all kinds of intermediate setups, e.g., a number of subsystems can be fully optimized, while for other subsystems the gas-phase density is only polarized in one freeze-and-thaw cycle and while for the remaining subsystems the frozen density of the isolated molecule is used. In addition, a number of additional options can be specified for each fragment. This provides a very flexible framework for performing multilevel simulations, in which different levels of accuracy are employed for different subsystems.[18,39,46] Such applications to large systems are further facilitated by the use of an efficient numerical integration scheme,[37] that makes applications possible also in the case of large frozen environments.

10.2.4. *Approximations to $T_s^{nadd}[\rho_I, \rho_{II}]$ and to $v_T[\rho_I, \rho_{II}]$*

Both the total energy bifunctional and the effective embedding potential contain a nonadditive kinetic-energy component that usually cannot be calculated exactly. For the performance of the FDE scheme, the choice of the approximation which is used for this nonadditive kinetic-energy component is of great importance.

Usually, the nonadditive kinetic energy is approximated in the form

$$\tilde{T}_s^{\mathrm{nadd}}[\rho_{\mathrm{I}}, \rho_{\mathrm{II}}] = \tilde{T}_s[\rho_{\mathrm{I}} + \rho_{\mathrm{II}}] - \tilde{T}_s[\rho_{\mathrm{I}}] - \tilde{T}_s[\rho_{\mathrm{II}}], \tag{10.2.12}$$

and the kinetic-energy component v_T of the embedding potential is approximated as

$$\tilde{v}_T[\rho_{\mathrm{I}}, \rho_{\mathrm{II}}](\boldsymbol{r}) = \left.\frac{\delta \tilde{T}_s[\rho]}{\delta \rho}\right|_{\rho=\rho_{\mathrm{tot}}(\boldsymbol{r})} - \left.\frac{\delta \tilde{T}_s[\rho]}{\delta \rho}\right|_{\rho=\rho_{\mathrm{I}}(\boldsymbol{r})}, \tag{10.2.13}$$

where the tilde is used to label approximate quantities, and $\tilde{T}_s[\rho]$ refers to some approximate kinetic-energy functional. Approximation to $T_s^{\mathrm{nadd}}[\rho_{\mathrm{I}}, \rho_{\mathrm{II}}]$ and to $v_T[\rho_{\mathrm{I}}, \rho_{\mathrm{II}}]$, that are of the form of Eq. (10.2.12) and Eq. (10.2.13) are denoted as *decomposable* approximations.[47] An overview of different approximate kinetic-energy functionals that can be used to construct such decomposable approximations can be found, e.g., in Ref. 48. Here, only a brief overview of the approximate functionals that are commonly used in combination with the FDE scheme is given.

The simplest approximation for the kinetic-energy functional, corresponding to the local-density approximation for exchange and correlation, is the Thomas–Fermi (TF) functional.[49,50] For the construction of GGA kinetic-energy functionals, the suggestion of Lee, Lee, and Parr[51] to use similar analytical forms for approximate kinetic-energy and exchange energy functionals can be applied. In a series of studies,[32,52,53] Wesolowski and co-workers compared the accuracy of different approximate kinetic-energy functionals—including the TF functional and several GGA functionals based on the suggestion of Lee, Lee, and Parr—for different hydrogen-bonded complexes. In particular, they investigated the hydrogen-bonded complexes $FH\cdots NCH$ (Ref. 52), $HCN\cdots H_2$ (Ref. 53) and a test set consisting of $(H_2O)_2$, $(HF)_2$, $(HCl)_2$, and $HF\cdots NCH$ (Ref. 32).

By comparing results of subsystem DFT (freeze-and-thaw) calculations to supermolecular KS-DFT calculations it was found that the functional that yields the most accurate interaction energies for the investigated complexes is the GGA functional which has the same analytic form of the enhancement factor as the exchange functional of Perdew and Wang[54] but should be reparametrized for the kinetic energy as described by Lembarki and Chermette. This functional is commonly dubbed PW91k.

However, the PW91k functional is only applicable if the interaction between the subsystems is small. In this case, the nonadditive kinetic energy T_s^{nadd} and the kinetic-energy component v_T of the embedding potential are small compared to the other contributions, so that rather crude approximations can be applied. For weakly interacting or hydrogen-bonded systems, the PW91k functional, therefore, leads to total electron densities which are very similar to those obtained from supermolecular KS-DFT calculations, as was shown by Kiewisch *et al.* by means of a topological analysis of the resulting electron densities.[34] This even holds for very strong hydrogen bonds, such as the one found in the complex $F–H–F^-$. But when going to complexes where the bond between the subsystems has a larger covalent character, such as ammonia borane (NH_3–BH_3), larger deviations in the electron densities occur, since the kinetic-energy component of the embedding potential is not sufficiently small anymore[55] (see also the overview given below in Sec. 10.3.3). Therefore, improved approximations to v_T have to be developed in order to describe covalent bonds (or even bonds with a significant covalent character) between subsystems adequately.

10.3. Development of improved approximations to $v_T[\rho_{\mathrm{I}}, \rho_{\mathrm{II}}]$

10.3.1. *Exact embedding potential*

An ideal starting point for the development of improved approximations to the kinetic-energy component of the embedding potential $v_T[\rho_{\mathrm{I}}, \rho_{\mathrm{II}}]$ is the knowledge of the *exact* $v_T[\rho_{\mathrm{I}}, \rho_{\mathrm{II}}]$—at least in specific limits or for certain systems. First, the exact behavior of $v_T[\rho_{\mathrm{I}}, \rho_{\mathrm{II}}]$ in specific limiting cases can be used as guidance when

constructing approximations by requiring that in these limits the exact $v_T[\rho_\mathrm{I}, \rho_\mathrm{II}]$ is recovered by the approximation. Second, the exact $v_T[\rho_\mathrm{I}, \rho_\mathrm{II}]$ can be used as a reference for assessing the quality and for identifying insufficiencies of a given approximation.

It is important to notice that in the FDE scheme, the accuracy of the obtained electron density and of the KS orbitals and orbital energies, which in turn determine most molecular properties, are directly related to the quality of the approximation that is used for $v_T[\rho_\mathrm{I}, \rho_\mathrm{II}]$, while an approximation to the nonadditive kinetic-energy $T_s^\mathrm{nadd}[\rho_\mathrm{I}, \rho_\mathrm{II}]$ is only required if the energy is needed. Since in general the quality of a certain approximation to $T_s^\mathrm{nadd}[\rho_\mathrm{I}, \rho_\mathrm{II}]$ is not related to the quality of the corresponding $v_T[\rho_\mathrm{I}, \rho_\mathrm{II}]$ (which can be obtained from $T_s^\mathrm{nadd}[\rho_\mathrm{I}, \rho_\mathrm{II}]$ by taking the functional derivative),[32] it is natural to directly consider $v_T[\rho_\mathrm{I}, \rho_\mathrm{II}]$ instead of $T_s^\mathrm{nadd}[\rho_\mathrm{I}, \rho_\mathrm{II}]$ when developing improved approximations.

In order to obtain $v_T[\rho_\mathrm{I}, \rho_\mathrm{II}]$, one needs to evaluate the functional derivative of the noninteracting kinetic energy $\frac{\delta T_s[\rho]}{\delta\rho}$ for two different densities, for $\rho_\mathrm{tot} = \rho_\mathrm{I} + \rho_\mathrm{II}$ and for ρ_I. This functional derivative, which is often referred to as *kinetic potential* in the literature, is through the Euler–Lagrange equation of DFT[56] related to the KS potential,[57,58]

$$\frac{\delta T_s[\rho]}{\delta\rho(\boldsymbol{r})} = -v_s[\rho](\boldsymbol{r}) + \mu^\rho. \tag{10.3.14}$$

In this expression, $v_s[\rho]$ denotes the potential for which the density ρ is the ground state density. Such a potential exists by definition for any v_s-representable density, and it is unique (up to a constant shift) according to the first Hohenberg-Kohn theorem. If the constant shift in the potential $v_s[\rho]$ is chosen such that it goes to zero at infinity, the constant μ^ρ equals the chemical potential, which can be identified with the energy of the highest-occupied KS orbital.[56,59] It should be noted that while $T_s[\rho]$ can be defined for any N-representable density, its functional derivative is only defined for v_s-representable densities.[57] In practice, different algorithms exist which allow one to determine this potential $v_s[\rho]$ for a given (v_s-representable) density.[60–63] The exact kinetic potentials determined according to Eq. (10.3.14) have been used in a number of studies to assess the quality of approximate kinetic-energy functionals in the context of orbital-free DFT.[48,64,65]

Using Eq. (10.3.14), the exact $v_T[\rho_\mathrm{I}, \rho_\mathrm{II}]$ can be obtained from[58]

$$\begin{aligned} v_T[\rho_\mathrm{I}, \rho_\mathrm{II}](\boldsymbol{r}) &= \left.\frac{\delta T_s[\rho]}{\delta\rho}\right|_{\rho=\rho_\mathrm{tot}(\boldsymbol{r})} - \left.\frac{\delta T_s[\rho]}{\delta\rho}\right|_{\rho=\rho_\mathrm{I}(\boldsymbol{r})} \\ &= v_s[\rho_\mathrm{I}](\boldsymbol{r}) - v_s[\rho_\mathrm{tot}](\boldsymbol{r}) + \Delta\mu, \end{aligned} \tag{10.3.15}$$

where $v_s[\rho_\mathrm{I}]$ denotes the potential for which ρ_I is the ground-state density, $v_s[\rho_\mathrm{tot}]$ is the potential for which ρ_tot is the ground-state density, and $\Delta\mu = \mu^{\rho_\mathrm{I}} - \mu^{\rho_\mathrm{tot}}$ only leads to a constant shift of the potential.

Equation (10.3.15) provides a recipe for the calculation of the exact $v_T[\rho_\mathrm{I}, \rho_\mathrm{II}]$ for a given pair of electron densities by reconstructing the KS potentials yielding the

densities ρ_{I} and ρ_{tot}. If one considers the density ρ_{tot} obtained from a supermolecular KS-DFT calculation, then $v_s[\rho_{\mathrm{tot}}](\boldsymbol{r})$ is known directly form this calculation. In this case, only $v_s[\rho_{\mathrm{I}}](\boldsymbol{r})$ has to be determined using a suitable algorithm for the reconstruction of the KS potential.[66]

However, the relation given in Eq. (10.3.15) only provides an implicit density functional, while an explicit density functional is needed in practical applications. Furthermore, the described procedure for the calculation of the exact $v_T[\rho_{\mathrm{I}}, \rho_{\mathrm{II}}]$ will only be computationally feasible for a few benchmark systems. Nevertheless, it can provide useful reference potentials for the development of improved (explicit) density-functionals to approximate $v_T[\rho_{\mathrm{I}}, \rho_{\mathrm{II}}]$. Furthermore, such a procedure can be useful for the construction of accurate embedding potentials within WFT-in-DFT embedding schemes.[67] It should further be noted that very similar approaches are used for the construction of local pseudopotentials, which are used in orbital-free DFT calculations.[68–70]

10.3.2. *Embedding potential in the limit of a small electron density of the active subsystem*

In order to identify deficiencies in the currently available approximations to $v_T[\rho_{\mathrm{I}}, \rho_{\mathrm{II}}]$, it can be very valuable to study the exact behavior of $v_T[\rho_{\mathrm{I}}, \rho_{\mathrm{II}}]$ in certain limiting cases. One such case is the limit that the density of the active subsystem ρ_{I} is small. This situation commonly rises at the frozen subsystem, in particular if the distance between the two subsystems is large. This limit has recently been investigated in detail in Refs. 58 and 47.

In this limit, $v_T[\rho_{\mathrm{I}}, \rho_{\mathrm{II}}]$ simplifies to (see Appendix A in Ref. 47),

$$\lim_{\rho_{\mathrm{I}}(\boldsymbol{r})\to 0} v_T[\rho_{\mathrm{I}}, \rho_{\mathrm{II}}](\boldsymbol{r}) = \left.\frac{\delta T_s[\rho]}{\delta\rho}\right|_{\rho=\rho_{\mathrm{II}}(\boldsymbol{r})}. \tag{10.3.16}$$

Using Eq. (10.3.14) one obtains[58]

$$\lim_{\rho_{\mathrm{I}}(\boldsymbol{r})\to 0} v_T[\rho_{\mathrm{I}}, \rho_{\mathrm{II}}](\boldsymbol{r}) = -v_s[\rho_{\mathrm{II}}](\boldsymbol{r}) + \mu^{\rho_{\mathrm{II}}}, \tag{10.3.17}$$

i.e., if ρ_{I} is small, the kinetic-energy component of the embedding potential is given by the KS potential that yields the frozen density ρ_{II}. To arrive at this expression, apart from the v_s-representability of all the involved densities no further assumptions have to be made.

If one additionally requires that the frozen density ρ_{II} is the ground-state density obtained for the isolated subsystem II, then $v_s[\rho_{\mathrm{II}}]$ is known and is given by the effective KS potential from the calculation on the isolated subsystem II. Therefore, one finds that in this case the kinetic-energy component cancels the other components of the embedding potentials, and the total embedding potential at the frozen subsystem is a constant,[58] i.e.,

$$\lim_{\rho_{\mathrm{I}}(\boldsymbol{r})\to 0} v_{\mathrm{eff}}^{\mathrm{emb}}[\rho_{\mathrm{I}}, \rho_{\mathrm{II}}](\boldsymbol{r}) = \mu^{\rho_{\mathrm{II}}} = \text{constant}. \tag{10.3.18}$$

In particular, near the nuclei of the frozen subsystem, $v_T[\rho_\mathrm{I}, \rho_\mathrm{II}]$ compensates the large nuclear attraction as well as the other components of the effective embedding potential.

However, this limit is not described correctly by all common approximations to $v_T[\rho_\mathrm{I}, \rho_\mathrm{II}]$. In particular, both the Thomas–Fermi (TF) approximation as well as the widely applied PW91k functional are not repulsive enough near the nuclei. This leads to a too attractive embedding potential near the nuclei of the frozen system, which can lead to severe problems in practical calculations. In particular, these problems show up when basis functions located on the frozen subsystem are included in the calculations (supermolecular basis set expansion[32]), which probe the embedding potential in regions where ρ_I should be small.

In Ref. 58, the consequences of the wrong behavior of the TF and the PW91k approximations in the considered limit were demonstrated for the model system $H_2O\cdots Li^+$ at large separations, where the Li^+ ion constitutes the frozen subsystem. It turned out that the incomplete compensation of the nuclear attraction of the lithium nucleus in the frozen subsystem leads to artificially low-lying orbitals on the frozen Li^+ subsystem. At large separations, the orbital energy of one of these orbitals even drops below the one of the highest occupied molecular orbital of the active subsystem, so that the self-consistent field iterations only converge if a non-aufbau solution is enforced.[58]

Even if the artificial lowering of the energies of unoccupied orbitals on the environment is not so severe that it results in a non-aufbau solution, it leads to serious problems if excitation energies are considered. In Ref. 58, this was shown for a cluster of the dye molecule aminocoumarin C151 surrounded by 30 solvent water molecules, which are treated as frozen environment. For the active subsystem consisting of the dye molecule, spurious low-lying virtual orbitals appear if basis functions on the frozen environment are included (see Fig. 10.3.1a). These virtual orbitals are rather diffuse orbitals which are located on the solvent environment, as is shown in Fig. 10.3.1b, and excitations to these spurious virtual orbitals will lead to spurious excitation energies.

One approach to address the incorrect behavior of common approximations to $v_T[\rho_\mathrm{I}, \rho_\mathrm{II}]$ is to go beyond decomposable approximations, i.e., approximations that are of the form of Eq. (10.2.13), and to introduce a *non-decomposable* approximation to $v_T[\rho_\mathrm{I}, \rho_\mathrm{II}]$, i.e., apply an approximation to $v_T[\rho_\mathrm{I}, \rho_\mathrm{II}]$ that is not based on an approximate kinetic-energy functional (cf. Eq. (10.2.13)). [a] In Ref. 58, a correction was proposed that can be added on top of a given decomposable approximation. This correction is designed such that in regions where ρ_II is significantly larger than

[a]Editors' note: In the present chapter, no distinction is made between different mathematical quantities: the function $v_T(\mathbf{r})$ and the bifunctional $v_T[\rho_I, \rho_{II}](\mathbf{r})$, i.e., unique mapping between the pair of functions $\rho_I(\mathbf{r})$ and $\rho_{II}(\mathbf{r})$ and the function $v_T(\mathbf{r})$ in 3D. For instance, RHS of Eq. 10.3.20 is not a bifunctional because it is not uniquely determined by ρ_I and ρ_{II}. It depends also on the third function $v_{II}^{nuc}(\mathbf{r})$. Although making such distinction is not crucial in numerical practice it is essential in formal considerations.

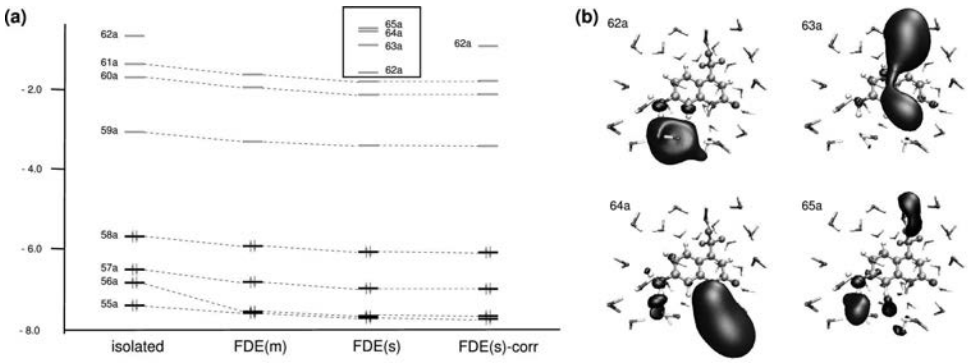

Fig. 10.3.1. Illustration of the consequences of the wrong behavior of the PW91k approximation at the frozen subsystem for the calculation of electronic excitation energies for a cluster of aminocoumarin C151 surrounded by 30 water molecules. (a) Orbitals energies (in eV) of the relevant orbitals. The orbital energies calculated for the isolated aminocoumarin C151 are shown as reference, together with those calculated using FDE (using the PW91k approximation for $v_T[\rho_\mathrm{I}, \rho_\mathrm{II}]$) not including [FDE(m)] and including basis functions on the frozen subsystem [FDE(s)]. Furthermore, the orbital energies calculated using FDE(s) and the correction proposed in Ref. 58 are shown [labeled FDE(s)-corr]. (b) Isosurface plots of the spurious virtual orbitals 62a to 65a obtained in the FDE(s) calculation. Reprinted with permission from Ref. 58. Copyright 2007 American Insitute of Physics.

ρ_I, i.e., at the frozen subsystem, the limit of Eq. (10.3.18) is explicitly enforced. For the case of the PW91k approximation, this leads to the non-decomposable approximation,

$$\tilde{v}_T[\rho_\mathrm{I}, \rho_\mathrm{II}](\boldsymbol{r}) = \tilde{v}_T^{\mathrm{PW91k}}[\rho_\mathrm{I}, \rho_\mathrm{II}](\boldsymbol{r}) + f\big(\rho_\mathrm{I}(\boldsymbol{r}), \rho_\mathrm{II}(\boldsymbol{r})\big) \cdot \tilde{v}_T^{\mathrm{corr}}[\rho_\mathrm{I}, \rho_\mathrm{II}](\boldsymbol{r}), \tag{10.3.19}$$

where $f\big(\rho_\mathrm{I}(\boldsymbol{r}), \rho_\mathrm{II}(\boldsymbol{r})\big)$ is a switching function that switches from 0 at the active subsystem to 1 at the frozen subsystem, and where the correction term is given by,

$$\tilde{v}_T^{\mathrm{corr}}[\rho_\mathrm{I}, \rho_\mathrm{II}](\boldsymbol{r}) = -\Bigg[v_\mathrm{II}^{\mathrm{nuc}}(\boldsymbol{r}) + \int \frac{\rho_\mathrm{II}(\boldsymbol{r'})}{|\boldsymbol{r} - \boldsymbol{r'}|} d\boldsymbol{r'} + \frac{\delta E_\mathrm{xc}[\rho]}{\delta \rho}\bigg|_{\rho=\rho_\mathrm{I}+\rho_\mathrm{II}} - \frac{\delta E_\mathrm{xc}[\rho]}{\delta \rho}\bigg|_{\rho=\rho_\mathrm{I}} + \tilde{v}_T^{\mathrm{PW91k}}[\rho_\mathrm{I}, \rho_\mathrm{II}](\boldsymbol{r})\Bigg], \tag{10.3.20}$$

i.e., it is chosen such that it cancels the other components of the embedding potential and the total embedding potential is thus zero when this correction term is switched on. Using this long-distance corrected approximation to $v_T[\rho_\mathrm{I}, \rho_\mathrm{II}]$, the problems with artificially low-lying unoccupied orbitals located on the frozen subsystem found for $H_2O\cdots Li^+$ at large separations can be overcome, and orbitals located on the frozen Li^+ are shifted to higher orbital energies. Furthermore, the problem with spurious low-lying virtual orbitals on the frozen environment found for aminocoumarin C151 surrounded by water molecules disappears (see also Fig. 10.3.1a).

However, it should be noted that the correction proposed in Ref. 58 has a number of disadvantages. First, the limit the correction enforces is only exact under the conditions given above for Eq. (10.3.18), i.e., if $\rho_{\mathrm{I}}(\boldsymbol{r}) \to 0$ and if ρ_{II} is the ground-state density obtained for the isolated subsystem II. In particular the latter condition will not be satisfied if the frozen density has been obtained in freeze-and-thaw iterations. Second, the chemical potential of subsystem II, $\mu^{\rho_{\mathrm{II}}}$, in Eq. (10.3.18) is set to zero, and therefore, the proposed correction will not be able to describe cases in which there should be a transfer of electron density from subsystem I to subsystem II, i.e., the partitioning of the electron density must a priori correspond to the correct dissociation limit. Third, the correction proposed in Ref. 58 is explicitly position-dependent, since the correction term in Eq. (10.3.20) contains the nuclear potential of subsystem II. Therefore, the approximation to $v_T[\rho_{\mathrm{I}}, \rho_{\mathrm{II}}]$ given in Eq. (10.3.19) is no explicit density functional, even though the positions and charges of the nuclei can in principle be deduced from the electron density. Furthermore, it cannot be obtained as a functional derivative of an approximation to the nonadditive kinetic-energy $T_s^{\mathrm{nadd}}[\rho_{\mathrm{I}}, \rho_{\mathrm{II}}]$.

The limit that the electron density ρ_{I} of subsystem I is small was also considered by Garcia Lastra *et al.* in Ref. 47. Starting from Eq. (10.3.16), they consider the case that ρ_{II} is a spin-compensated two-electron density. For such a system, the exact noninteracting kinetic energy is given by the von Weizsäcker kinetic-energy functional,[71] so that one obtains,

$$\lim_{\rho_{\mathrm{I}}(\boldsymbol{r})\to 0} v_T[\rho_{\mathrm{I}}, \rho_{\mathrm{II}}](\boldsymbol{r}) = \left.\frac{\delta \tilde{T}_s^{\mathrm{vW}}[\rho]}{\delta\rho}\right|_{\rho=\rho_{\mathrm{II}}(\boldsymbol{r})} = \frac{1}{8}\frac{\left|\nabla\rho_{\mathrm{II}}(\boldsymbol{r})\right|^2}{\rho_{\mathrm{II}}(\boldsymbol{r})^2} - \frac{1}{4}\frac{\nabla^2\rho_{\mathrm{II}}(\boldsymbol{r})}{\rho_{\mathrm{II}}(\boldsymbol{r})}, \quad (10.3.21)$$

for $N_{\mathrm{II}} = \int \rho_{\mathrm{II}}(\boldsymbol{r})d\boldsymbol{r} = 2$. The von Weizsäcker functional also gives the correct limit near the nuclear cusps, where the electron density is dominated by a single $1s$-type orbital. Therefore, the above expression should also be applicable near the nuclei of the frozen subsystem. Based on this exact limit given by Eq. (10.3.21), Garcia Lastra *et al.* develop a non-decomposable approximation (dubbed *non-decomposable approximant using first and second derivatives of* ρ, NDSD) to $v_T[\rho_{\mathrm{I}}, \rho_{\mathrm{II}}]$ which is given by,[47]

$$\tilde{v}_T^{\mathrm{NDSD}}[\rho_{\mathrm{I}}, \rho_{\mathrm{II}}](\boldsymbol{r}) = \tilde{v}_T^{\mathrm{TF}}[\rho_{\mathrm{I}}, \rho_{\mathrm{II}}](\boldsymbol{r}) + f\big(\rho_{\mathrm{II}}(\boldsymbol{r}), \nabla\rho_{\mathrm{II}}(\boldsymbol{r})\big) \left.\frac{\delta \tilde{T}_s^{\mathrm{vW}}[\rho]}{\delta\rho}\right|_{\rho=\rho_{\mathrm{II}}(\boldsymbol{r})}, \quad (10.3.22)$$

where $f\big(\rho_{\mathrm{II}}(\boldsymbol{r}), \nabla\rho_{\mathrm{II}}(\boldsymbol{r})\big)$ is a switching function depending on the reduced density gradient and the electron density of subsystem II that is designed such that it is 1 in regions close to the nuclei of the frozen subsystem, where Eq. (10.3.21) can be expected to hold, and that is 0 in region where this is not the case.

In contrast to the correction proposed in Ref. 58, the NDSD approximant of Ref. 47 is an explicit density functional, and it can be obtained as the functional derivative of a corresponding approximation to the nonadditive kinetic energy

$T_s^{\mathrm{nadd}}[\rho_{\mathrm{I}}, \rho_{\mathrm{II}}]$. As is shown in Ref. 47 for a test set containing a diverse set of weakly interacting and hydrogen-bonded systems, the NDSD approximation leads for all considered molecules to more accurate complexation-induced dipole moments than both the TF and the PW91k approximations.

However, also the NDSD approximation exhibits some limitations. For $H_2O\cdots Li^+$ at large separations, it is not able to completely remove the problem with too low-lying unoccupied orbitals located on the frozen Li^+ subsystem, but it only shifts these orbitals to slightly higher energies so that the separation at which a non-aufbau solution is obtained is increased. This is because even though Eq. (10.3.21) is exact for the frozen two-electron system Li^+, this limit is only enforced near the nucleus and not in all regions where ρ_{I} is small. Furthermore, due to the form of the NDSD approximant, the zeroth-order TF term stays finite near the nuclei, although it should be switched off.[47]

10.3.3. *Assessment of approximations to $v_T[\rho_I, \rho_{II}]$ for the description of covalent bonds*

To assess the quality of a given approximation to $v_T[\rho_{\mathrm{I}}, \rho_{\mathrm{II}}]$ one can compare the electron densities of a subsystem DFT calculation, in which the electron densities of both subsystems are determined iteratively in freeze-and-thaw iterations, to those from a supermolecular KS-DFT calculation.[32] If in the subsystem DFT calculation the supermolecular basis set expansion is used, and if a GGA exchange–correlation functional is applied, all differences to the supermolecular KS-DFT results can be attributed to the approximations used for the kinetic-energy component of the embedding potential $v_T[\rho_{\mathrm{I}}, \rho_{\mathrm{II}}]$. Note that if the electron densities are compared, all differences can be attributed to the approximation used for $v_T[\rho_{\mathrm{I}}, \rho_{\mathrm{II}}]$. In contrast, if interaction energies are compared both the approximation used for $v_T[\rho_{\mathrm{I}}, \rho_{\mathrm{II}}]$ and the one used for $T_s^{\mathrm{nadd}}[\rho_{\mathrm{I}}, \rho_{\mathrm{II}}]$ contribute to the observed errors. Therefore, it is preferable to investigate errors in the electron density, since such a strategy allows it to isolate the errors that originate from the approximation that is applied for $v_T[\rho_{\mathrm{I}}, \rho_{\mathrm{II}}]$.

While most studies compare an integrated measure for the differences in the electron density, such as differences in the dipole moments[31,32,47] or the integral of the absolute difference density,[72] only few studies have performed a spatially-resolved comparison of the electron densities.[34,52,55] A useful tool for the spatially-resolved comparison of the electron densities from subsystem DFT and supermolecular KS-DFT calculations is a topological analysis according to the theory of atoms-in-molecules,[73] that has first been applied to the analysis of electron densities obtained from subsystem DFT by Kiewisch *et al.*[34]

In Ref. 34, the electron densities obtained for $HOH\cdots F^-$, F–H–F^-, and the nucleic acid base pair adenine-thymine were analyzed, and it was found that if the PW91k kinetic-energy functional is used to approximate $v_T[\rho_{\mathrm{I}}, \rho_{\mathrm{II}}]$, accurate electron densities can be obtained for the considered hydrogen-bonded systems. This

is true even for F–H–F$^-$, which contains a very strong hydrogen bond. For this complex, subsystem DFT yields an almost symmetrical electron-density distribution, even though a non-symmetric partitioning into an HF and an F$^-$ subsystem is employed.

A similar analysis was performed in Ref. 55, where coordination compounds in which the bonding has a significant covalent character were considered. First, ammonia borane NH_3BH_3 was considered, divided into an NH_3 and a BH_3 subsystem, which are connected by a dative bond. This bond is actually weaker than the one found in F–H–F$^-$, but due to its larger covalent character more difficult to describe in subsystem DFT. While subsystem DFT using the PW91k kinetic-energy functional to approximate $v_T[\rho_\mathrm{I}, \rho_\mathrm{II}]$ yields overall a reasonable electron density, some of the features of the electron density obtained from a supermolecular KS-DFT calculation are not reproduced correctly.[55]

Second, the tetrahedral complex $TiCl_4$ was considered, partitioned into a $TiCl_3^+$ and a Cl^- subsystem. For this complex, large problems are observed in the subsystem DFT calculation if the PW91k approximation is employed. In the calculation in which Cl^- is the active subsystem, a spurious charge transfer to the frozen $TiCl_3^+$ subsystem occurs, and in the subsequent calculation in which the $TiCl_3^+$ subsystem is active, a non-aufbau solution has to be enforced. These difficulties are due to the incorrect behavior of the available GGA approximations to $v_T[\rho_\mathrm{I}, \rho_\mathrm{II}]$ at the frozen subsystem that was discussed in Sec. 10.3.2. If the correction suggested in Ref. 58 is applied, these problems disappear and the subsystem DFT calculations converge to aufbau solutions for both subsystems. Furthermore, the electron density obtained from subsystem DFT are in this case qualitatively correct, even though there are quantitative differences.

Third, Ref. 55 considered the octahedral complex $Cr(CO)_6$, divided into a subsystem containing the chromium atom and a subsystem consisting of the CO ligands. In contrast to $TiCl_4$, the bonding between the ligands and the metal is to a large part of electrostatic nature, $Cr(CO)_6$ is a prototypical example of a metal complex in which π-backdonation plays a significant role, i.e., it presents an even more challenging test case for the available approximations to $v_T[\rho_\mathrm{I}, \rho_\mathrm{II}]$. In the subsystem DFT calculations using the PW91k approximation, no aufbau solution could be obtained. This situation is not changed by applying the correction of Ref. 58, even though in this case the number of unoccupied orbitals that are too low in energy is decreased. If one considers the electron density corresponding to this non-aufbau solution, it is found that there are large qualitative deviations to the density obtained from a supermolecular KS-DFT calculation, i.e., the available approximations to $v_T[\rho_\mathrm{I}, \rho_\mathrm{II}]$ are not able to describe the bonding in $Cr(CO)_6$.

These results of Ref. 55 show that the limit investigated in Ref. 58 and 47 is—even though it was initially investigated in a very different context—of great relevance for a description of covalent bonds. In particular, the correction suggested in Ref. 58 turns out to be essential in order to be able to obtain an aufbau solution in

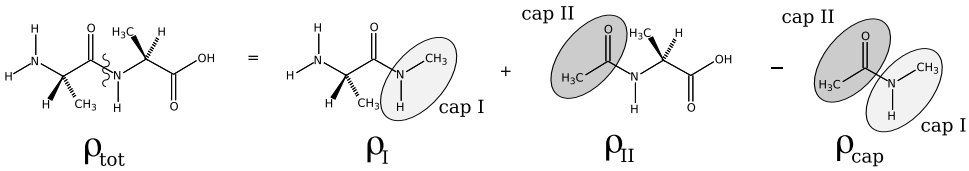

Fig. 10.4.2. Partitioning using capping groups employed in the 3-FDE scheme illustrated for dialanine. The total electron density is obtained as $\rho_{\mathrm{tot}}(\boldsymbol{r}) = \rho_{\mathrm{I}}(\boldsymbol{r}) + \rho_{\mathrm{II}}(\boldsymbol{r}) - \rho_{\mathrm{cap}}(\boldsymbol{r})$. This partitioning can be easily generalized to larger capping groups and to a larger number of subsystems.

the case of $TiCl_4$, and is found to at least work in the correct direction for $Cr(CO)_6$. Similar results can be expected for the NDSD approximant of Ref. 47, even though it has not been tested for coordination compounds or other systems with a covalent bonds between subsystems yet. Nevertheless, none of the available approximations to $v_T[\rho_{\mathrm{I}}, \rho_{\mathrm{II}}]$ is currently able to describe the considered coordination compounds adequately.

A similar picture emerges from a study[74] on the family of triatomic noble gas–goldhalides that feature a gold–noble gas bond of varying strengths.[75,76] None of the currently available functionals was able to provide a quantitatively correct description of the magnitude of charge transfer from the noble gas to the goldhalide unit. Better approximations to $v_T[\rho_{\mathrm{I}}, \rho_{\mathrm{II}}]$ that are able to utilize the subtle information od the atomic shell structure contained in the density of the heavy atom will be needed to tackle such cases.

10.4. Introduction of capping groups

10.4.1. *Three-partition frozen-density embedding*

For the efficient computational treatment of biochemical processes a subsystem description of proteins, in which individual amino acid residues can be used as subsystems, is very desirable. However, as discussed above the currently available approximations to $v_T[\rho_{\mathrm{I}}, \rho_{\mathrm{II}}]$ are not applicable to subsystems connected by covalent bonds, which is required for such a description. Even though the developments outlined in the previous section are promising, improved approximations cannot be expected to lead to a satisfactory description of covalent bonds between subsystems in the near future. Therefore, other approaches have to be developed.

One possibility to allow for a description of subsystems connected by covalent bonds is the introduction of capping groups, in a similar way as it is done within combined quantum mechanics/molecular mechanics (QM/MM) schemes.[77,78] In this way, it is possible to circumvent the insufficiencies of the available approximations to $v_T[\rho_{\mathrm{I}}, \rho_{\mathrm{II}}]$ since it is no longer necessary to describe the covalent bonds connecting subsystems using an approximate kinetic-energy functional. Instead, these bonds are replaced by bonds to newly introduced capping groups, which are treated within the individual subsystems.

Applying this strategy, a molecule is cut into two subsystems across some arbitrary covalent bond, and two capping groups are included in each of the two subsystems. These capping groups are chosen such that the electronic structure of the bond that is cut is preserved as well as possible. The two capping groups are joined to form a "capping molecule", and the electron density of this capping molecule is subtracted from the densities of the subsystems to correct for the introduced capping groups. The total electron density is thus partitioned according to

$$\rho_{\mathrm{tot}}(\boldsymbol{r}) = \rho_{\mathrm{I}}(\boldsymbol{r}) + \rho_{\mathrm{II}}(\boldsymbol{r}) - \rho_{\mathrm{cap}}(\boldsymbol{r}), \tag{10.4.23}$$

where ρ_{I} and ρ_{II} are the electron densities of subsystems I and II (including the corresponding capping groups), respectively, and ρ_{cap} is the electron density of the capping molecule. This partitioning is illustrated in Fig. 10.4.2 for the example of a dialanine molecule. The use of such a partitioning was first suggested for the description of proteins by Zhang and coworkers,[12] who employed such a partitioning to calculate the electron density of proteins from that of the individual subsystems, which were each treated as isolated molecules (*molecular fractionation with conjugate caps*, MFCC scheme). However, this MFCC scheme does not include any effect of the neighboring amino acid residues and of the protein environment on the individual subsystems, so that it can only be considered as a first approximation to an adequate subsystem treatment of proteins.

The use of the above partitioning of the total density in the FDE scheme was first proposed by Casida and Wesolowski.[79] However, they did not present an implementation of this three-partition FDE (3-FDE) scheme, and their formalism did not ensure that the total electron density is positive. This positivity of the total electron density is ensured in the 3-FDE formalism presented in Ref. 80 by requiring that inside a suitably defined "cap region", the density of the active subsystem I equals the density of the cap molecule. It is important to introduce such a constraint, since in partitioning of the total electron density given in Eq. (10.4.23) the density of the cap molecule is subtracted, so that regions of unphysical negative electron density could otherwise be obtained. Starting from the total DFT energy written as a functional of the densities of the three densities ρ_{I}, ρ_{II}, and ρ_{cap}], $E[\rho_{\mathrm{I}}, \rho_{\mathrm{II}}, \rho_{\mathrm{cap}}]$, one can derive a set of one-electron equations for the KS orbitals of subsystem I in the presence of a given frozen density ρ_{II} and a given cap density ρ_{cap} by minimizing $E[\rho_{\mathrm{I}}, \rho_{\mathrm{II}}, \rho_{\mathrm{cap}}]$ with respect to ρ_{I} under the constraint that $\rho_{\mathrm{I}}(\boldsymbol{r}) = \rho_{\mathrm{cap}}(\boldsymbol{r})$ inside a cap region $V_{\mathrm{I}}^{\mathrm{cap}}$. This leads to the KSCED-like equations[80]

$$\left[-\frac{\nabla^2}{2} + v_{\mathrm{eff}}^{\mathrm{KSCED}}[\rho_{\mathrm{I}}, \rho_{\mathrm{II}}, \rho_{\mathrm{cap}}](\boldsymbol{r})\right] \phi_i^{(\mathrm{I})}(\boldsymbol{r}) = \epsilon_i \, \phi_i^{(\mathrm{I})}(\boldsymbol{r}); \quad i = 1, \ldots, N_{\mathrm{I}}/2, \tag{10.4.24}$$

in which the effective potential is now given by

$$v_{\mathrm{eff}}^{\mathrm{KSCED}}[\rho_{\mathrm{I}}, \rho_{\mathrm{II}}, \rho_{\mathrm{cap}}](\boldsymbol{r}) = \begin{cases} v_{\mathrm{eff}}^{\mathrm{KS}}[\rho_{\mathrm{I}}](\boldsymbol{r}) + v_{\mathrm{eff}}^{\mathrm{emb}}[\rho_{\mathrm{I}}, \rho_{\mathrm{II}}](\boldsymbol{r}) & \text{for} \quad \boldsymbol{r} \notin V_{\mathrm{I}}^{\mathrm{cap}} \\ v_{\mathrm{cap}}[\rho_{\mathrm{I}}, \rho_{\mathrm{cap}}](\boldsymbol{r}) & \text{for} \quad \boldsymbol{r} \in V_{\mathrm{I}}^{\mathrm{cap}}. \end{cases} \tag{10.4.25}$$

Outside the cap region $V_{\mathrm{I}}^{\mathrm{cap}}$, the effective potential contains—similar as in the case of the conventional two-partition FDE scheme—the KS potential $v_{\mathrm{eff}}^{KS}[\rho_{\mathrm{I}}]$ of the isolated subsystem I as well as an effective embedding potential that reads,

$$\begin{aligned} v_{\mathrm{eff}}^{\mathrm{emb}}[\rho_{\mathrm{I}},\rho_{\mathrm{II}},\rho_{\mathrm{cap}}](\boldsymbol{r}) = v_{\mathrm{II}}^{\mathrm{nuc}}(\boldsymbol{r}) - v_{\mathrm{cap}}^{\mathrm{nuc}}(\boldsymbol{r}) + \int \frac{\rho_{\mathrm{II}}(\boldsymbol{r'}) - \rho_{\mathrm{cap}}(\boldsymbol{r'})}{|\boldsymbol{r}-\boldsymbol{r'}|} d\boldsymbol{r'} \\ + \left.\frac{\delta E_{\mathrm{xc}}[\rho]}{\delta\rho}\right|_{\rho=\rho_{\mathrm{I}}+\rho_{\mathrm{II}}-\rho_{\mathrm{cap}}} - \left.\frac{\delta E_{\mathrm{xc}}[\rho]}{\delta\rho}\right|_{\rho=\rho_{\mathrm{I}}} \\ + v_T[\rho_{\mathrm{I}},\rho_{\mathrm{II}},\rho_{\mathrm{cap}}], \end{aligned} \tag{10.4.26}$$

where the kinetic-energy component is given by,

$$v_T[\rho_{\mathrm{I}},\rho_{\mathrm{II}},\rho_{\mathrm{cap}}] = \left.\frac{\delta T_s[\rho]}{\delta\rho}\right|_{\rho=\rho_{\mathrm{I}}+\rho_{\mathrm{II}}-\rho_{\mathrm{cap}}} - \left.\frac{\delta T_s[\rho]}{\delta\rho}\right|_{\rho=\rho_{\mathrm{I}}}. \tag{10.4.27}$$

Inside the cap region $V_{\mathrm{I}}^{\mathrm{cap}}$, the effective potential is given by a cap potential $v_{\mathrm{cap}}[\rho_{\mathrm{I}},\rho_{\mathrm{cap}}]$, which arises from the constraint that the electron density of the active subsystem I, ρ_{I}, should be equal to the density of the cap molecule ρ_{cap}. This cap potential has to be determined such that this constraint is satisfied. In practice, different algorithms can be applied to achieve this, and in Ref. 80 the algorithm proposed by van Leeuwen and Baerends[60] has been employed, i.e., the cap potential is updated iteratively according to,

$$v_{\mathrm{cap}}^{\mathrm{new}}(\boldsymbol{r}) = \frac{\rho_{\mathrm{I}}^{\mathrm{old}}(\boldsymbol{r})}{\rho_{\mathrm{cap}}(\boldsymbol{r})}\, v_{\mathrm{cap}}^{\mathrm{old}}(\boldsymbol{r}), \tag{10.4.28}$$

where $\rho_{\mathrm{I}}^{\mathrm{old}}$ is the electron density of subsystem I obtained using the cap potential $v_{\mathrm{cap}}^{\mathrm{old}}$ in a certain iteration.

To assess the accuracy of the 3-FDE scheme, one can compare the electron densities obtained from 3-FDE calculations, in which the densities of both subsystems have been optimized (possibly using a number of freeze-and-thaw iterations) to those from supermolecular KS-DFT calculations. So far, for the cap molecule the electron density calculated for the isolated molecule has always been used. Test calculations on different dipeptides show that the 3-FDE scheme can accurately model both the polarization of a subsystem due to its environment as well as the effects of hydrogen bonding.[80] However, since the electron density in the cap region is constrained, the distribution of the electrons between the subsystems is also fixed, and a polarization of the bond between the subsystems cannot be accounted for. This problem could possibly be addressed by a more adequate choice of the density of the cap molecule that accounts for this polarization.

10.4.2. *Application to the description of proteins*

The 3-FDE scheme can be easily generalized to an arbitrary number of subsystems.[80] In the general case of n_{sub} subsystems and n_{cap} capping molecules, the

total electron density is given by,

$$\rho_{\mathrm{tot}}(\boldsymbol{r}) = \sum_{i=1}^{n_{\mathrm{sub}}} \rho_i(\boldsymbol{r}) - \sum_{j=1}^{n_{\mathrm{cap}}} \rho_j^{\mathrm{cap}}(\boldsymbol{r}), \tag{10.4.29}$$

where ρ_i is the electron density of subsystem i (including the corresponding capping groups) and ρ_j^{cap} is the electron density of cap molecule j. This leads to a subsystem DFT formulation that allows it to treat proteins, and in which the individual amino acid residues can be used as subsystems.

In practical applications of such a subsystem DFT treatment, one faces the rather tedious task of defining the individual subsystems and of determining the atomic coordinates of the atoms in the capping groups. Furthermore, a large number of individual calculations have to be performed for each cap molecule and for each subsystem. To automate these tasks, the scripting framework PyAdf can be employed.[81]

To illustrate the accuracy of the proposed subsystem DFT treatment of a protein, Ref. 80 includes calculations performed for the protein ubiquitin [see Fig. 10.4.3(a)]. For this protein consisting of 76 amino acids, a full supermolecular KS-DFT calculation is still possible, so that the electron densities obtained from a subsystem treatment can be compared to the one from a supermolecular KS-DFT calculation. In the subsystem treatment, different levels of approximation can be applied. First, the electron densities obtained from calculations for the isolated molecules can be applied for all subsystems, corresponding to the MFCC scheme. Second, the electron density of each of the subsystems can be optimized in a 3-FDE calculation in which the embedding potential of the isolated fragments is included for each subsystem, and finally, the electron densities of all subsystems can be optimized iteratively in freeze-and-thaw cycles. The difference in the total electron density with respect to the supermolecular KS-DFT calculation is shown in Fig. 10.4.3 for calculations employing these different levels of approximations. It can be seen that already the simplest possible 3-FDE description improves significantly over the MFCC scheme, and that a very accurate electron density can be obtained if five freeze-and-thaw cycles are applied.

The subsystem DFT description based on the 3-FDE scheme is particularly suited for applications where focus can be placed on a small part of a protein, such as, for instance, an active site of an enzyme, or for the calculation of rather localized molecular properties. In this case, only a few subsystems have to be treated accurately by employing 3-FDE with several freeze-and-thaw cycles, while for the electron density of subsystems further away from the region of interest, a simple approximation using the densities obtained from calculations for isolated molecules as it is used in the MFCC scheme can be used. Such a strategy is similar to the one chosen in applications of FDE for modeling solvent effects on molecular properties.[17,26,37–39]

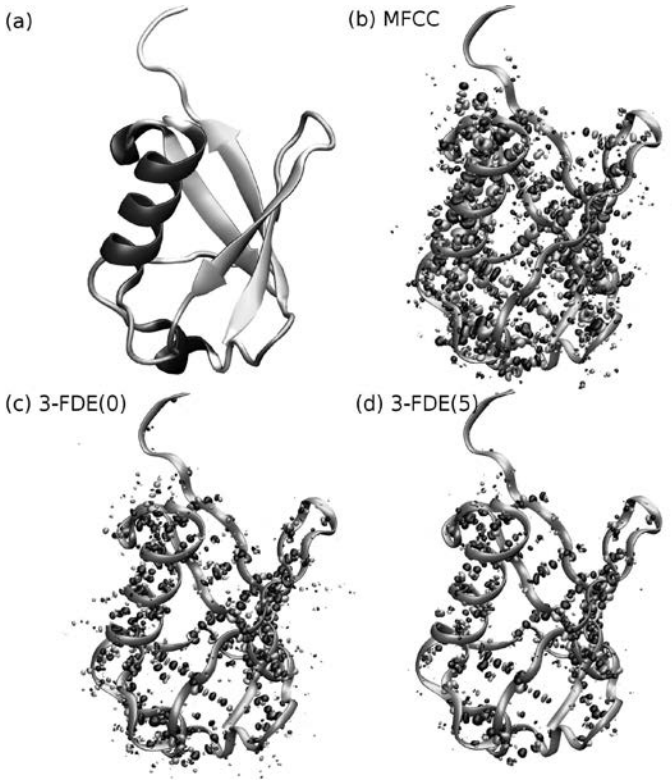

Fig. 10.4.3. (a) Cartoon representation of the secondary structure of ubiquitin. (b-d) Isosurface plots (contour value 0.002 a.u.) of the difference densities between (b) the MFCC calculation, in which all subsystems are treated as isolated fragments, (c) the 3-FDE(0) calculation, in which the embedding potential of the isolated fragments is included for each subsystem, and (d) the 3-FDE(5) calculation, in which five freeze-and-thaw iterations are performed, and the conventional supermolecular KS-DFT calculation for ubiquitin. Reprinted with permission from Ref. 80. Copyright 2008 American Insitute of Physics.

10.5. Conclusions and outlook

For the computational treatment of a number of interesting chemical problems, in particular for studying biochemical processes and for investigating condensed phase chemistry, a subsystem DFT treatment is advantageous. Such a subsystem treatment not only allows an efficient computational treatment of large systems, but it also facilitates the analysis of the computational results by offering a picture in terms of the system's chemical building blocks. Furthermore, a subsystem treatment makes it possible to focus on certain parts of a system, and to employ accurate (relativistic) wave-function based methods for certain parts of the system.[46]

A subsystem DFT treatment based on the FDE scheme introduced by Wesolowski and Warshel[16] requires the use of approximate density-functionals for the nonadditive kinetic energy $T_s^{\mathrm{nadd}}[\rho_{\mathrm{I}}, \rho_{\mathrm{II}}]$ and the corresponding component of

the embedding potential $v_T[\rho_\mathrm{I}, \rho_\mathrm{II}]$. So far, approximations based on GGA kinetic energy functionals have been used in practical applications of the FDE scheme. While those approximations are sufficiently accurate for weak interactions and hydrogen bonds, they are not adequate for the description of covalent bonds between subsystems. However, a treatment of subsystems connected by covalent bonds is essential for studying, e.g., large biological molecules or transition metal catalysts. Therefore, the development of subsystem DFT schemes applicable to such systems presents an important challenge. One possible approach to achieve this goal is the development of improved approximations to the kinetic-energy component of the embedding potential.

A promising strategy for the development of improved approximations to $v_T[\rho_\mathrm{I}, \rho_\mathrm{II}]$ is the investigation of exact limits, a route that has also been successful for the development of non-empirical approximations to the exchange–correlation functional (see, e.g., Ref. 82). One such exact limit for $v_T[\rho_\mathrm{I}, \rho_\mathrm{II}]$ that has been studied recently is the limit that the electron density of the active subsystem ρ_I is small, and different ways to improve the description of this limit have been suggested.[47,58] However, while these approximations improve the description in a number of cases, they both do not strictly incorporate the exact limit. Nevertheless, it has been shown that an improved description of the embedding potential at the frozen subsystem leads to an improved description of covalent bonds in some cases, even though there are still severe deficiencies, as has been shown for representative coordination compounds.[55]

Therefore, further improvements of the approximations to $v_T[\rho_\mathrm{I}, \rho_\mathrm{II}]$ are necessary. From the recent developments reviewed here, some possible directions for future work emerge. First, it appears that the previously used decomposable approximations, which are derived from an approximate kinetic-energy functional, have reached their limits, and that non-decomposable approximations, which approximate $T_s^\mathrm{nadd}[\rho_\mathrm{I}, \rho_\mathrm{II}]$ or $v_T[\rho_\mathrm{I}, \rho_\mathrm{II}]$ directly, are more promising. Second, for an accurate description of covalent bonds it might be necessary to go beyond the framework initially suggested by Wesolowski and Warshel,[16] i.e., to abandon the restriction that an explicit density functional that only locally depends on the densities ρ_I and ρ_II should be used for approximating $v_T[\rho_\mathrm{I}, \rho_\mathrm{II}]$. An example of such an approximation is the position-dependent correction proposed in Ref. 58. In analogy to the development of approximate exchange–correlation functionals, one could imagine to climb the next rugs of Jacob's ladder[83] for approximations to $v_T[\rho_\mathrm{I}, \rho_\mathrm{II}]$ by introducing dependencies on the occupied KS orbitals of subsystem I. A further step could be to introduce also a dependency on the KS orbitals of the frozen subsystem II, at the price of abandoning the idea of an "orbital-free" embedding scheme.

A different line of development could arise by applying nonlocal approximate kinetic-energy functionals, such as the ones developed by Carter and coworkers,[84–86] to approximate $v_T[\rho_\mathrm{I}, \rho_\mathrm{II}]$. These functionals are designed to describe the linear-

response of the uniform electron gas correctly, and have successfully been applied in simulations of solid state systems using orbital-free DFT, even for materials with significant covalent bonding, such as silicon. In particular, these functional have recently been reformulated in real-space,[87,88] which allows for an application in molecular DFT codes.

However, since the development of improved approximations to $v_T[\rho_\mathrm{I}, \rho_\mathrm{II}]$ is challenging, also other approaches that make a subsystem description possible in which subsystems are connected by covalent bonds are needed. Therefore, a generalization of the FDE scheme to three partitions has been developed that treats covalent bonds between subsystems by introducing capping groups. This allows it to treat subsystems connected by covalent bonds, even though additional approximations have to be introduced. Even though this generalization has been initially applied to proteins which are partitioned into individual amino acids, the method is applicable to arbitrary (bio)-molecules and arbitrary partitioning

Altogether, significant progress has been made towards a description of covalent bonds within subsystem DFT, both on the side of the development of improved approximations to the kinetic-energy component of the embedding potential, and by developing ways to circumvent the problems in the currently available approximations.

Acknowledgments

The authors would like to acknowledge extensive and fruitful discussions with Tomasz Wesolowski (University of Geneva), in particular on the issues discussed in Sec. 10.3.2, and thank the Netherlands Organization for Scientific Research (NWO) for financial support via a Rubicon scholarship (C.R.J.) and the Vici program (L.V.). C.R.J. further thanks the DFG-Center for Functional Nanostructures.

References

1. M. Reiher, Ed., *Atomistic Approaches in Modern Biology.* vol. 268, *Topics in Current Chemistry.* (Springer, Berlin, 2007).
2. R. R. Schrock, *Angew. Chem., Int. Ed.* **47**, 5512 (2008).
3. G.-J. Kroes, *Science* **321**, 794 (2008).
4. P. Huang and E. A. Carter, *Annu. Rev. Phys. Chem.* **59**, 261 (2008).
5. J. VandeVondele, M. Krack, F. Mohamed, M. Parrinello, T. Chassaing, and J. Hutter, *Comput. Phys. Commun.* **167**, 103 (2005).
6. C. Ochsenfeld, J. Kussmann, and D. S. Lambrecht. *Linear-Scaling Methods in Quantum Chemistry*, In *Reviews in Computational Chemistry*, vol. 23, pp. 1–82. Wiley-VCH, New York, (2007).
7. C. Herrmann, J. Neugebauer, and M. Reiher, *New J. Chem.* **1**, 818 (2007).
8. Ch. R. Jacob and M. Reiher, *J. Chem. Phys.* **130**, 084106 (2009).
9. P. Cortona, *Phys. Rev. B* **44**, 8454 (1991).
10. M. Iannuzzi, B. Kirchner, and J. Hutter, *Chem. Phys. Lett.* **421**, 16 (2006).

11. F. Shimojo, R. K. Kalia, A. Nakano, and P. Vashishta, *Comput. Phys. Commun.* **167**, 151 (2005).
12. D. W. Zhang and J. Z. H. Zhang, *J. Chem. Phys.* **119**, 3599 (2003).
13. D. G. Fedorov and K. Kitaura, *J. Phys. Chem. A.* **111**, 6904 (2007).
14. R. P. A. Bettens and A. M. Lee, *J. Phys. Chem. A.* **110**, 8777 (2006).
15. H. M. Netzloff and M. A. Collins, *J. Chem. Phys.* **127**, 134113 (2007).
16. T. A. Wesolowski and A. Warshel, *J. Phys. Chem.* **97**, 8050 (1993).
17. J. Neugebauer, M. J. Louwerse, E. J. Baerends, and T. A. Wesolowski, *J. Chem. Phys.* **122**, 094115 (2005).
18. Ch. R. Jacob, J. Neugebauer, and L. Visscher, *J. Comput. Chem.* **9**, 1011 (2008).
19. N. Govind, Y. A. Wang, and E. A. Carter, *J. Chem. Phys.* **110**, 7677 (1999).
20. T. Klüner, N. Govind, Y. A. Wang, and E. A. Carter, *Phys. Rev. Lett.* **86**, 5954 (2001).
21. T. Klüner, N. Govind, Y. A. Wang, and E. A. Carter, *J. Chem. Phys.* **116**, 42 (2002).
22. P. Huang and E. A. Carter, *J. Chem. Phys.* **125**, 084102 (2006).
23. S. Sharifzadeh, P. Huang, and E. Carter, *J. Phys. Chem. C.* **112**, 4649 (2008).
24. S. Sharifzadeh, P. Huang, and E. A. Carter, *Chem. Phys. Lett.* **470**, 347 (2009).
25. T. A. Wesolowski. *One-electron equations for embedded electron density: challenge for theory and practical payoffs in multilevel modelling of complex polyatomic systems.* In ed. J. Leszczynski, *Computational Chemistry: Reviews of Current Trends*, vol. 10. (World Scientific, Singapore, 2006).
26. Ch. R. Jacob, J. Neugebauer, L. Jensen, and L. Visscher, *Phys. Chem. Chem. Phys.* **8**, 2349 (2006).
27. T. A. Wesolowski and J. Weber, *Chem. Phys. Lett.* **248**, 71 (1996).
28. A. Lembarki and H. Chermette, *Phys. Rev. A.* **50**, 5328 (1994).
29. T. A. Wesolowski, Y. Ellinger, and J. Weber, *J. Chem. Phys.* **108**, 6078 (1998).
30. T. A. Wesolowski and F. Tran, *J. Chem. Phys.* **118**, 2072 (2003).
31. Ch. R. Jacob, T. A. Wesolowski, and L. Visscher, *J. Chem. Phys.* **123**, 174104 (2005).
32. T. A. Wesolowski, *J. Chem. Phys.* **106**, 8516 (1997).
33. T. A. Wesolowski, *J. Am. Chem. Soc.* **126**, 11444 (2004).
34. K. Kiewisch, G. Eickerling, M. Reiher, and J. Neugebauer, *J. Chem. Phys.* **128**, 044114 (2008).
35. T. A. Wesolowski, *Chem. Phys. Lett.* **311**, 87 (1999).
36. T. Wesolowski and A. Warshel, *J. Phys. Chem.* **98**, 5183 (1994).
37. J. Neugebauer, Ch. R. Jacob, T. A. Wesolowski, and E. J. Baerends, *J. Phys. Chem. A* **109**, 7805 (2005).
38. J. Neugebauer, M. J. Louwerse, P. Belanzoni, T. A. Wesolowski, and E. J. Baerends, *J. Chem. Phys.* **123**, 114101 (2005).
39. R. E. Bulo, Ch. R. Jacob, and L. Visscher, *J. Phys. Chem. A* **112**, 2640 (2008).
40. P. Cortona, *Phys. Rev. B* **46**, 2008 (1992).
41. P. Cortona and A. Villafiorita Monteleone, *J. Phys.: Condens. Matter* **8**, 8983 (1996).
42. P. Cortona, A. Villafiorita Monteleone, and P. Becker, *Int. J. Quantum Chem.* **56**, 831 (1995).
43. W. N. Mei, L. L. Boyer, M. J. Mehl, M. M. Ossowski, and H. T. Stokes, *Phys. Rev. B* **61**, 11425 (2000).
44. M. M. Ossowski, L. L. Boyer, M. J. Mehl, and H. T. Stokes, *Phys. Rev. B* **66**, 224302 (2002).
45. P. Vashishta, R. K. Kalia, and A. Nakano, *J. Phys. Chem. B* **110**, 3727 (2006).
46. A. S. P. Gomes, Ch. R. Jacob, and L. Visscher, *Phys. Chem. Chem. Phys.* **10**, 5353 (2008).

47. J. M. Garcia Lastra, J. W. Kaminski, and T. A. Wesolowski, *J. Chem. Phys.* **129**, 074107 (2008).
48. Y. A. Wang and E. A. Carter. *Orbital-free kinetic-energy density functional theory*, In ed. S. D. Schwartz, *Theoretical Methods in Condensed Phase Chemistry*, pp. 117–184. (Kluwer, Dordrecht, 2000).
49. L. H. Thomas, *Proc. Cambridge Philos. Soc.* **23**, 542 (1927).
50. E. Fermi, *Z.Phys.* **48**, 73 (1928).
51. H. Lee, C. Lee, and R. G. Parr, *Phys. Rev. A* **44**, 768 (1991).
52. T. A. Wesolowski, H. Chermette, and J. Weber, *J. Chem. Phys.* **105**, 9182 (1996).
53. T. A. Wesolowski and J. Weber, *Int. J. Quantum Chem.* **61**, 303 (1997).
54. J. P. Perdew. *Unified theory of exchange and correlation beyond the local density approximation*, In eds. P. Ziesche and H. Eschrig, *Electronic Structure of Solids*, pp. 11–20. (Akademie Verlag, Berlin, 1991).
55. S. Fux, K. Kiewisch, Ch. R. Jacob, J. Neugebauer, and M. Reiher, *Chem. Phys. Lett.* **461**, 353 (2008).
56. R. G. Parr and W. Yang, *Density-Functional Theory of Atoms and Molecules*. (Oxford University Press, Oxford, 1989).
57. S. Liu and P. W. Ayers, *Phys. Rev. A* **70**, 022501 (2004).
58. Ch. R. Jacob, S. M. Beyhan, and L. Visscher, *J. Chem. Phys.* **126**, 234116 (2007).
59. J. P. Perdew, R. G. Parr, M. Levy, and J. L. Balduz Jr., *Phys. Rev. Lett.* **49**, 1691 (1982).
60. R. van Leeuwen and E. J. Baerends, *Phys. Rev. A* **49**, 2421 (1994).
61. Q. Zhao, R. C. Morrison, and R. G. Parr, *Phys. Rev. A* **50**, 2138 (1994).
62. F. Colonna and A. Savin, *J. Chem. Phys.* **110**, 2828 (1999).
63. E. S. Kadantsev and M. J. Scott, *Phys. Rev. A* **69**, 012502 (2004).
64. R. A. King and N. C. Handy, *Phys. Chem. Chem. Phys.* **2**, 5049 (2000).
65. J.-D. Chai and J. D. Weeks, *Phys. Rev. B* **75**, 205122 (2007).
66. S. Fux, Ch. R. Jacob, J. Neugebauer, L. Visscher, and M. Reiher, *J. Chem. Phys.* **132**, 164101 (2010).
67. O. Roncero, M. P. de Lara-Castells, P. Villarreal, F. Flores, J. Ortega, M. Paniagua, and A. Aguado, *J. Chem. Phys.* **129**, 184104 (2008).
68. B. Zhou, Y. A. Wang, and E. A. Carter, *Phys. Rev. B* **69**, 125109 (2004).
69. B. Zhou and E. A. Carter, *J. Chem. Phys.* **122**, 184108 (2005).
70. C. Huang and E. A. Carter, *Phys. Chem. Chem. Phys.* **10**, 7109 (2008).
71. C. F. von Weizsäcker, *Z.Phys.* **96**, 431(1935).
72. Y. A. Bernard, M. Dulak, J. W. Kaminski, and T. A. Wesolowski, *J. Phys. A: Math. Theor.* **41**, 055302 (2008).
73. R. F. W. Bader, *Atoms in Molecules: A Quantum Theory*. (Clarendon Press, Oxford, 1990).
74. S. M. Beyhan, A. W. Götz, Ch. R. Jacob, and L. Visscher, *J. Chem. Phys.* **132**, 044114 (2010).
75. S. A. Cooke and M. C. L. Gerry, *J. Am. Chem. Soc.* **126**, 17000 (2004).
76. L. Belpassi, I. Infante, F. Tarantelli, and L. Visscher, *J. Am. Chem. Soc.* **130**, 1048 (2008).
77. M. J. Field, P. A. Bash, and M. Karplus, *J. Comput. Chem.* **11**, 700 (1990).
78. I. Antes and W. Thiel, *J. Phys. Chem. A* **103**, 9290 (1999).
79. M. E. Casida and T. A. Wesolowski, *Int. J. Quantum Chem.* **96**, 577 (2004).
80. Ch. R. Jacob and L. Visscher, *J. Chem. Phys.* **128**, 155102 (2008).
81. Ch. R. Jacob, R. E. Bulo, and L. Visscher. *PyADF — A Scripting Framework for Quantum Chemistry.*, in preparation (2009).

82. J. P. Perdew, A. Ruzsinszky, J. Tao, V. N. Staroverov, G. E. Scuseria, and G. I. Csonka, *J. Chem. Phys.* **123**, 062201 (2005).
83. J. P. Perdew and K. Schmidt. *Jacob's Ladder of density Functional Approximations for the Exchange-Correlation Energy*, In eds. V. van Doren, C. van Alsenoy, and P. Geerlings, *Density Functional Theory and Its Application to Materials*, pp. 1–20. (American Institute of Physics, Melville, New York, 2001).
84. Y. A. Wang, N. Govind, and E. A. Carter, *Phys. Rev. B* **58**, 13465 (1998).
85. Y. A. Wang, N. Govind, and E. A. Carter, *Phys. Rev. B* **60**, 16350 (1999).
86. B. Zhou, V. L. Ligneres, and E. A. Carter, *J. Chem. Phys.* **122**, 044103 (2005).
87. N. Choly and E. Kaxiras, *Solid State Commun.* **121**, 281 (2002).
88. G. S. Ho, V. L. Ligneres, and E. A. Carter, *Phys. Rev. B* **78**, 045105 (2008).